



# Synchrotron-based phase-sensitive imaging of leaves grown from magneto-primed seeds of soybean

A. Fatima,<sup>a\*</sup> S. Kataria,<sup>b\*</sup> L. Baghel,<sup>b</sup> K. N. Guruprasad,<sup>b</sup> A. K. Agrawal,<sup>c</sup> B. Singh,<sup>c</sup> P. S. Sarkar,<sup>c</sup> T. Shripathi<sup>a</sup> and Y. Kashyap<sup>c</sup>

<sup>a</sup>UGC-DAE, Consortium for Scientific Research, Indore (MP), India, <sup>b</sup>School of Life Sciences, DAVV, Khandwa Road, Indore (MP), India, and <sup>c</sup>Neutron and X-ray Physics Division, Bhabha Atomic Research Center, Trombay, Mumbai, India.  
 \*Correspondence e-mail: anees349@gmail.com, sunita\_kataria@yahoo.com

Received 2 July 2016

Accepted 6 October 2016

Edited by A. Momose, Tohoku University, Japan

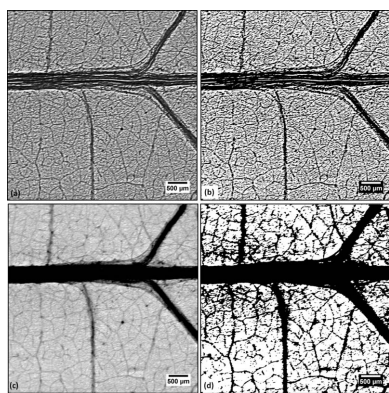
**Keywords:** phase-contrast imaging; phase retrieval; micro-imaging; soybean.

**Supporting information:** this article has supporting information at journals.iucr.org/s

Experiments were conducted to study the effects of static magnetic fields (SMFs) on the venation network of soybean leaves using the synchrotron-based X-ray micro-imaging technique. The seeds of soybean (*Glycine max*, variety JS-335) were pretreated with different SMFs from 50 to 300 mT in steps of 50 mT for 1 h. The phase-contrast images obtained showed that, as the strength of the SMF increased, the area, width of the midrib, area of the midrib and minor vein of the middle leaflets of third trifoliate leaves also increased up to the SMF strength of 200 mT (1 h) and decreased thereafter. Quantification of the major conducting vein also showed the differences in the major and minor vein structures of the soybean leaves as compared with control leaves. Further, the phase-retrieval technique has been applied to make the segmentation process easy and to quantify the major and minor veins in the venation network. The width and area of midrib enhancement by pre-treatment with SMF implies an enhancement in the uptake of water, which in turn causes an increased rate of photosynthesis and stomatal conductance.

## 1. Introduction

The effects of magnetic fields on the functioning of biological systems is being actively studied (Belyavskaya, 2004). There are studies showing the positive effects of magnetic flux and exposure time on plant characteristics such as seed germination, growth (Muraji *et al.*, 1998; Reina & Pascual, 2001) and reducing the adverse effects of pathogenic microbes (Galland & Pazur, 2005) and abiotic stresses like salinity, drought and UV-B (Anand *et al.*, 2012; Kataria *et al.*, 2015; Baghel *et al.*, 2015, 2016). The mechanism of the interaction of magnetic fields with biological systems has been explained by magneto-reception theory which accounts for the reaction of plants to DC/static fields and alternating magnetic fields (Camps-Raga *et al.*, 2009; Shine *et al.*, 2011a,b; Shine & Guruprasad, 2012). There are two mechanisms for magneto-reception: the radical pair mechanism (RPM) and ion cyclotron resonance (ICR). These two mechanisms provide a theoretical framework for model guided investigations of plant magneto-reception. The RPM modulates chemical reaction rates, while modulation of the transport rate is caused by the ICR mechanism (Galland & Pazur, 2005). This ion cyclotron resonance centers on the fact that ions should circulate in a plane perpendicular to an external magnetic field with larmor frequencies (Galland & Pazur, 2005). Magnetic field enhanced seed germination has been observed by many researchers (Florez *et al.*, 2007; Shine *et al.*, 2011b; Thomas *et al.*, 2013). Magnetic fields have positively influenced the growth of plants by increasing the lengths



of shoots and roots. Magnetic field pretreated seeds increased the water uptake and conductivity of the cellular membrane compared with untreated seeds (Reina & Pascual, 2001).

The architectural properties of a leaf are related to its functional aspects. The leaf venation network determines the photosynthetic activity and plays an important role in the transport phenomena in leaves and hydraulic functions (Brodrribb *et al.*, 2007, 2010; Sack & Holbrook, 2006; Walls, 2011). Apart from the function of transporting water and solutes, venation provides mechanical support to the leaf structure (Roth-Nebelsick *et al.*, 2001). The major conducting vein (1°) or midrib and the adjoining (2°) vein are the lower-order veins which provide fast and long-distance water transport while the higher-order veins are responsible for the local dispersion of water. The structure and dimensions of these lower-order veins are therefore important for the hydraulic efficiency of a leaf. The diameters of the veins are the factors which contribute to the final hydraulic conductance (Brodrribb *et al.*, 2007). To obtain information about the efficiency of the venation pattern, investigation of the leaf hydraulic conductance with fine structure of veins is necessary (Roth-Nebelsick *et al.*, 2001).

So far, studies reporting on the venation network have been carried out on chemically cleared leaf images. This process is not accurate because sometimes only the major vein could be quantified. Quantification of leaf venation networks has always been difficult and laborious. Analyses of complex vascular systems in plants were carried out using manual methods (Zimmerman & Tomlinson, 1966). Recently, with the developments of advanced imaging software, the study of the venation of whole images of the leaf is possible along with image quantification (Price *et al.*, 2011; Brodersen *et al.*, 2011). The advent of synchrotron sources and their various advantages in imaging have led to the developments in X-ray imaging of leaves (Blonder *et al.*, 2012). Quantification of venation networks for studying resource distribution is performed using semi-automatic image analysis software (Price *et al.*, 2011; Rolland-Lagan *et al.*, 2009). The segmentation of leaves images after phase retrieval of X-ray phase-contrast images will ease the quantification methods for two-dimensional and three-dimensional images.

In phase-contrast imaging, the incident X-rays that are transmitted through the sample have induced phase shifts. These phase shifts are observed as intensity variations at the detector, which is placed at a sufficiently large distance in the case of propagation-based phase-contrast imaging (Snigirev *et al.*, 1995; Wilkins *et al.*, 1996). There exists a quantitative relationship between the induced phase shifts and the contrast recorded at the detector placed in the Fresnel region. The method of retrieving the phase shifts induced by the sample is an inverse problem (Paganin *et al.*, 2002). The inverse problem can be addressed by capturing phase-contrast radiographs in the propagation-based set-up. The data set used for phase retrieval is single-distance or multi-energy and multi-distance for samples composed of multiple materials. The phase-contrast images are used as input to measure the phase distribution in the phase-retrieval process. This process of

retrieving the phase map of the object can be accomplished by selecting a suitable phase-retrieval algorithm.

There have been phase-retrieval studies on polymer composites, which are weakly absorbing materials (Xu *et al.*, 2010). Typically, phase-contrast methods and phase-retrieval studies are applied to soft material with low-*Z* elements. Phase-retrieval algorithms have the advantage of segmenting different phases of the object. Leaves are also composed of low-*Z* elements and phase-retrieval studies using the *ANKA* plugin in *ImageJ ANKA* software are presented (Weitkamp *et al.*, 2011). This plugin implements the algorithm with the assumptions that the sample has a homogeneous composition and monochromatic radiation is used (Paganin *et al.*, 2002). This algorithm has been applied in studies of various samples (Mokso *et al.*, 2013). There are also studies using this algorithm with a polychromatic source (Zápražný *et al.*, 2013). Phase-retrieval study of plant microstructure is also reported with the implementation of the Paganin algorithm through *X-TRACT* software (Mayo *et al.*, 2010). Phase-retrieval studies using this algorithm have relaxations in the basic assumptions shown by theoretical predictions and experimental results (Myers *et al.*, 2007).

The leaf vasculature plays crucial roles in the transport and mechanical support to the plants. Studies of the venation network under the influence of environmental effects like UV-exclusion have also been made (Fatima *et al.*, 2016). Previous reports (Shine *et al.*, 2011b; Baghel *et al.*, 2016) on soybean suggested that static magnetic field (SMF) pretreatment increases the leaf area, biomass accumulation and rate of photosynthesis. However, the effects of SMF pretreatment on the leaf architecture and venation network in soybean has not been studied yet. Thus, the aim of the present study was to investigate the effect of different strengths of SMF (50–300 mT) on the architecture and venation network in the soybean leaves, which finally supports plant growth, using the X-ray micro-imaging technique.

## 2. Materials and methods

Breeder seeds of soybean [*Glycine max* (L.) Merr. variety JS-335] were obtained from the Directorate of Soybean Research, Indore, India. Experiments were conducted on the terrace of the Department of Life Sciences, Devi Ahilya University, Indore, India (latitude 22°43'N) during August to October 2015. The SMF treated and untreated seeds of soybean variety JS-335 were treated with recommended fungicides, *viz.* Bevistin and Diathane M at 2 g kg<sup>-1</sup> seeds, and then these seeds were inoculated with *Rhizobium* culture (National Fertilizer limited, New-Delhi, India) 3 g kg<sup>-1</sup> seeds before sowing.

## 3. Magnetic field generation

An electromagnetic field generator (Testron EM-20, Testron India, Delhi, India) with a variable horizontal magnetic field strength of 50–500 mT and a gap of 5 cm between pole pieces was fabricated (Vashisth & Nagarajan, 2008). The pole pieces

were cylindrical in shape with a diameter of 9 cm and a length of 16 cm. The number of turns per coil was 3000 and the resistance of the coil was 16 Ω. A DC power supply (80 V/10 A) with a continuously variable output current was used for the electromagnet. A digital Gauss meter (Model DGM-30, Testron India) operating on the principle of the Hall effect monitored the field strength produced in the pole gap. The probe, made of indium arsenide crystals, was encapsulated in a non-magnetic sheet of 5 × 4 × 1 mm and could measure 0–2 T with a full-scale range in increments of 5 mT. The local geomagnetic field was less than 60 μT and the direction of the local geomagnetic field was north to south.

#### 4. Magnetic treatment

Soybean seeds were exposed to a magnetic field of 50–300 mT for 1 h in a cylindrical-shaped sample holder with a capacity of 42 cm<sup>3</sup>, made from a non-magnetic thin transparent plastic sheet. One-hundred visibly sound, mature and healthy seeds held in the plastic container were placed between the poles of the electromagnet under a uniform magnetic field treated for durations of 1 h. The required strength of the magnetic field was obtained by regulating the current in the coils of the electromagnet. The variation in the magnetic field strength from the center to the end of the pole was about 0.5% in the horizontal direction and 1.4% in the vertical direction at magnetic field strengths of 150 and 200 mT. The temperature during the course of seed exposure was 298 K.

#### 5. Leaf area and photosynthesis

Plants were sampled randomly in triplicate (*n* = 3) from all the treatments at 45 days after the emergence of seedlings (DAE). The area of the third trifoliate leaf was measured using a portable laser leaf area meter CID-202 scanning planimeter (CID Inc., USA). The rate of photosynthesis ( $P_N$  μmol CO<sub>2</sub> m<sup>-2</sup> s<sup>-1</sup>) and stomatal conductance ( $g_s$ , mmol H<sub>2</sub>O m<sup>-2</sup> s<sup>-1</sup>) were recorded using a portable infrared gas analyser (LI-6200, LICOR Inc., Lincoln, USA) in intact plants grown in plastic bags at midday between 1100 and 1200 hrs. Photosynthetic measurements were made under ambient temperature and CO<sub>2</sub> concentration on clear days for each treatment from 0 mT to 300 mT, the photosynthetic photon flux density was 1300–1600 μmol m<sup>-2</sup> s<sup>-1</sup>, the air flow 500 μmol s<sup>-1</sup> and the CO<sub>2</sub> concentration 350–380 p.p.m.

#### 6. Phase-contrast imaging technique

The Imaging beamline (BL4) at the Indus-2 synchrotron radiation source was used to carry out the imaging experiments (Agrawal *et al.*, 2015; Fatima *et al.*, 2016). A Si(111) double-crystal monochromator was used to select the suitable energy in the range 8–35 keV available from the broad white band of electromagnetic radiation. The synchrotron-based in-line phase-contrast imaging set-up consisted of motorized precision translation stages *x*, *y* and *z* and a rotation stage. The sample holder had a centrally fitted chuck for holding the

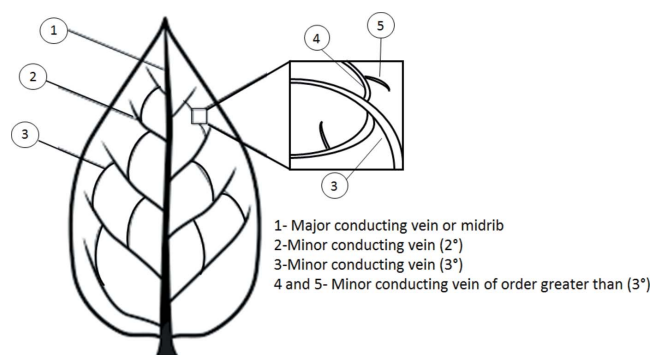


**Figure 1** Labelled diagram of soybean leaf showing the major vein (midrib) and the minor veins of the higher order.

samples. The high-resolution X-ray microscope with 3 μm resolution (20 μm thick YAG-Ce scintillator, 4× objective and PCO-2000 CCD camera) was used for image capture.

Leaves from all the magnetic field treatments were pressed flat and dried for two days at room temperature. The whole middle leaflet of third trifoliate leaves was mounted in a rectangular metallic frame and phase-contrast images were acquired for the tip, middle and base regions in each leaf. Phase-contrast images of all the leaves were acquired at 10 keV energy and 430 mm sample-to-detector distance. Flat-field and dark-field images were also acquired to correct the sample image.

Quantification of the midrib vein in phase-contrast images of the tip, middle and base area of leaves was carried out using *ImageJ* (Rasband, 2012). The midrib width was found in the direction perpendicular to the length at six places at fixed intervals. The average width of the midrib was obtained for the tip, middle and base region and an average value for the leaf was then calculated. Fig. 1 shows a labelled diagram of a soybean leaf showing the major vein (midrib) and the minor veins of higher order.

For the phase-retrieval method, phase-contrast images of the middle region of all the leaves were used as the input. The process was accomplished using the *ANKA* plugin in *ImageJ*.  $\delta$  and  $\beta$  values were obtained for cellulose (C<sub>6</sub>H<sub>10</sub>O<sub>5</sub>)<sub>*n*</sub> which is the dominating material in leaves with density 1.5 g cm<sup>-3</sup>. Values of  $\delta = 3.3129 \times 10^{-6}$  and  $\beta = 5.6256 \times 10^{-9}$  for cellulose at 10 keV were taken from the Henke database ([http://henke.lbl.gov/optical\\_constants/getdb2.html](http://henke.lbl.gov/optical_constants/getdb2.html)). The signal-to-noise ratio was calculated for phase-contrast and phase-retrieved images by dividing the mean value by the standard deviation of the image pixel obtained with the image histogram. The phase-retrieved images of all the leaves of 1624 × 2040 pixel size were segmented using the threshold operation in *Image J*. These segmented images were then used to obtain the area of the midrib and 2° minor veins.

#### 7. Statistical analysis

All data are presented in triplicate (*n* = 3) for recording all the parameters studied. The data are expressed as means ± standard error and analyzed by the analysis of variance

(ANOVA) followed by *post hoc* Newman–Keuls multiple comparison test ( $*P < 0.05$ ,  $**P < 0.01$ ,  $***P < 0.001$ ) using *Prism4* software for Windows (GraphPad Software, La Jolla, California, USA).

## 8. Results and discussion

Fig. 2(a) shows the dramatic change in area of the third trifoliolate leaf of soybean plants raised after treatment of different SMF strengths (0–300 mT for 1 h). The area of the third trifoliolate leaves of soybean (45 days after emergence) increases with the increase in dose strength of SMF treatment as compared with the untreated controls (Fig. 2a). The enhancement in the middle leaflets of third trifoliolate leaves of soybean was maximum at 200 mT (1 h); after that a decrease was noticed at the higher SMF strengths (250 and 300 mT for 1 h) (Fig. 2b). The maximum enhancement of 37.5% was found in the area of the middle leaflets of third trifoliolate leaves at 200 mT, and 36.5% increase was found at 150 mT. SMF pretreatment of 200 mT (1 h) significantly enhanced the net rate of photosynthesis and stomatal conductance in the middle leaflets of third trifoliolate leaves of soybean (Figs. 2c and 2d). It caused 34% increase in the net rate of photosynthesis and

32% increase in stomatal conductance as compared with untreated controls (Figs. 2c and 2d). Enhancement of growth in terms of leaf area after the SMF pre-treatment (200 mT for 1 h) has been previously reported in soybean and maize (Shine & Guruprasad, 2012; Shine *et al.*, 2011b; Baghel *et al.*, 2016), while the increase in rate of photosynthesis along with stomatal conductance in soybean after pretreatment with different strength of SMFs (50 mT to 300 mT for 1 h) was reported first in this study.

In the present study, images were obtained for the middle leaflets of third trifoliolate leaves of soybean emerged after pretreatment of different SMF strength (0–300 mT for 1 h) (Fig. 3). The venation architecture of soybean leaves was investigated for the effects of magneto-priming. The leaf vein architecture limits photosynthesis *via* its effect on hydraulic efficiency (Brodrribb *et al.*, 2007). The stomatal conductance plays a critical role in regulating the fluxes of both water and CO<sub>2</sub>, and therefore affects plant water-use efficiency (Galmés *et al.*, 2011). Our findings of synchrotron micro-imaging experiments agree with the photosynthesis and stomatal conductance results (Figs. 2c and 2d). Data presented here on soybean confirm the stimulatory effect of magnetic fields on the performance of seedlings. Quantitative examination of

phase-contrast images shows variation in midrib width in the leaves emerged after pretreatment of seeds with SMF strengths of 50–300 mT for 1 h along with the control (0 mT) (Figs. 3a–3g). A significant difference of 41% was found in the area of midrib and minor veins, and 20% in the width of the midrib was observed in third trifoliolate leaves of soybean (Figs. 4a and 4b). The width of the midrib obtained for all the imaged middle leaflets (Figs. 3a–3g) shows a maximum midrib width value for 200 mT middle leaflet third trifoliolate leaves of soybean. On further increasing the magnetic field strength from 250 to 300 mT the width of the midrib was less compared with 200 mT SMF treatments. A large extent enhancement in the vascular region near the midrib was observed in the phase-contrast images of leaves emerged after 200 mT SMF (1 h) pre-treatment (Fig. 3e) as compared with the control (Fig. 3a). The vascular regions in control and 200 mT leaflets images are shown by the blue rectangles. The dose response experiment of leaves grown with magneto-primed soybean seeds of different strength thus shows maximum enhancement for the midrib in the 200 mT leaf for exposure of 1 h. There is a specific combination of magnetic field strength

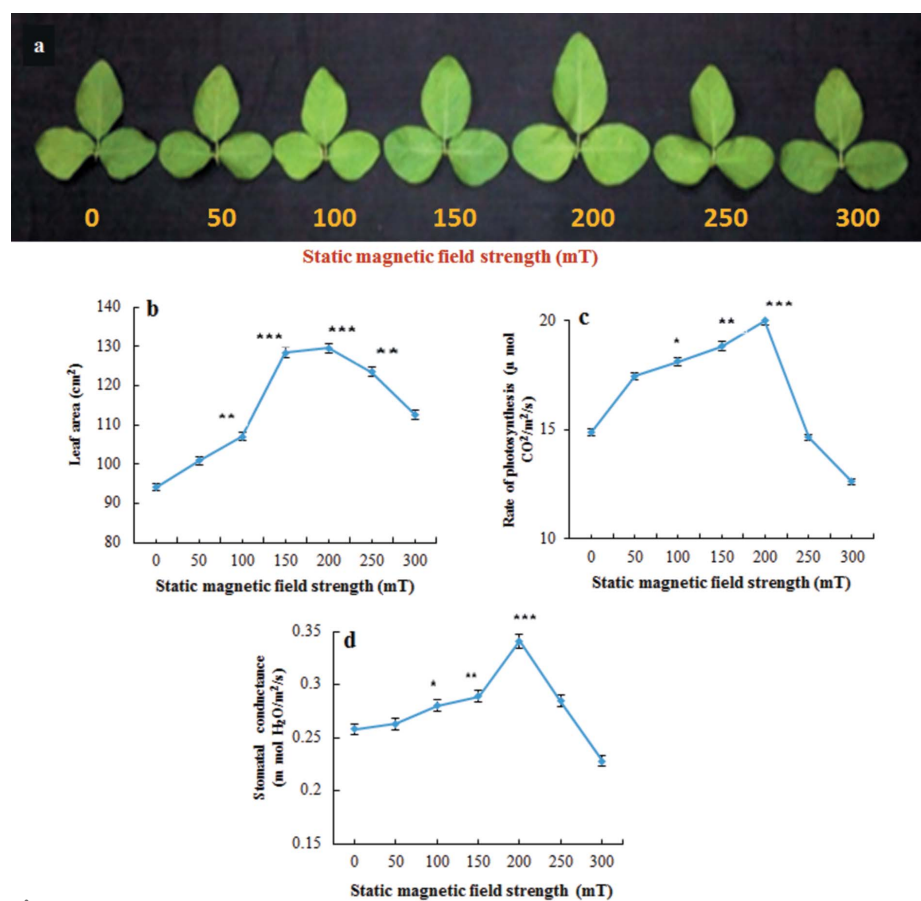
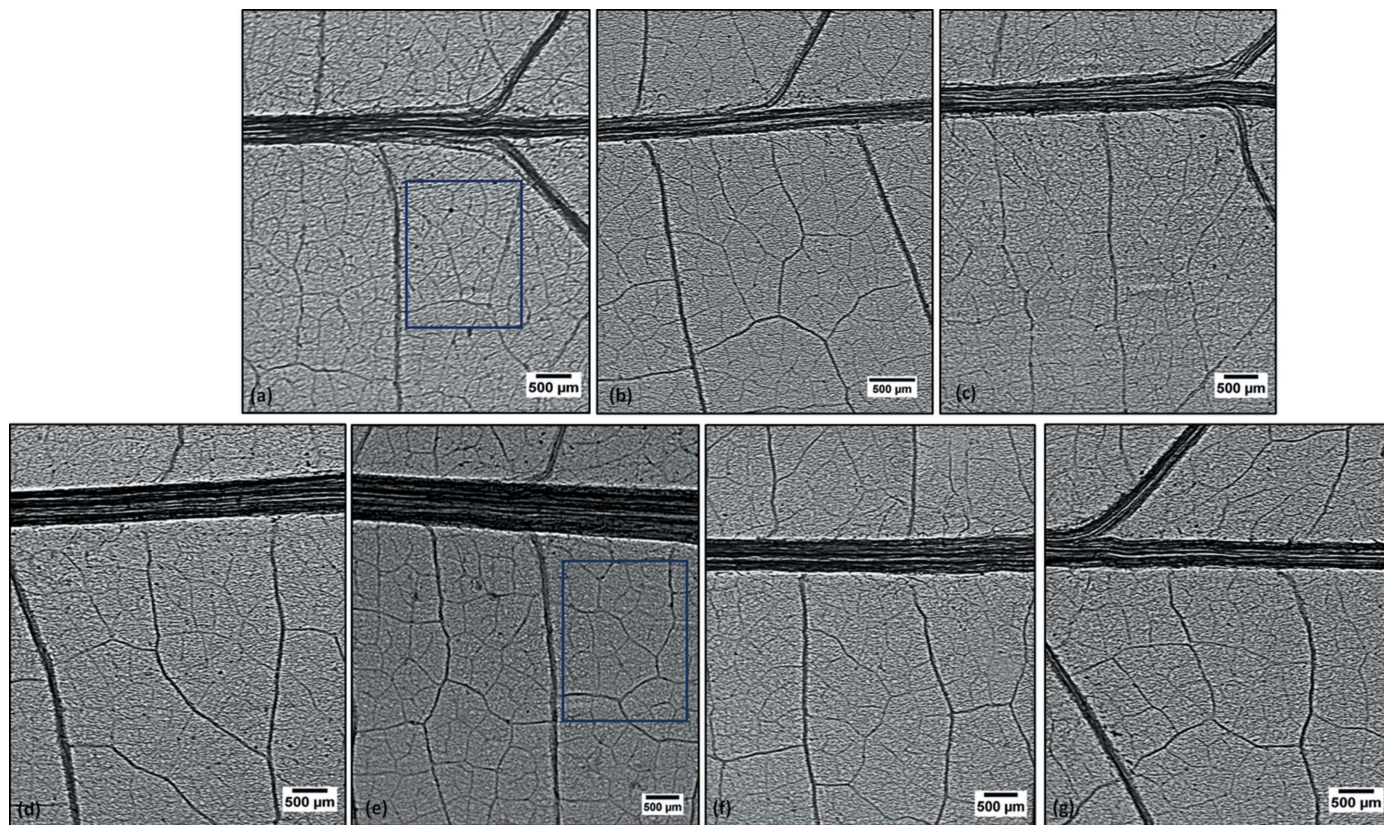


Figure 2

(a) Photograph of leaves, (b) area of leaves, (c) rate of photosynthesis and (d) stomatal conductance of third trifoliolate leaves of soybean plants emerged after pre-treatment of seeds with different SMF strengths (0–300 mT). The error bars indicate  $\pm$  standard error for the mean. The values presented are significantly different at ( $**P < 0.01$ ,  $***P < 0.001$ ) from untreated seeds (Newman–Keuls multiple comparison test).



**Figure 3**  
 (a)–(g) Phase-contrast images of the middle region of leaves of soybean plants emerged after pre-treatment of seeds with different SMF strength (0–300 mT in steps of 50 mT) showing midrib enhancement for 200 mT field strength. The vascular regions (marked with a blue rectangle) near the midrib in the control and 200 mT leaves show an enhancement for the 200 mT leaves.

and exposure time duration for which plant characteristics are enhanced (Shine *et al.*, 2011b).

The leaf hydraulic efficiency which is responsible for transport of water, nutrients and carbon in plants was enhanced by SMF pretreatment and the effects are displayed in the leaf venation architecture. These innovations resulted in large leaves with thicker major veins for mechanical support and a high vein length per unit area enabling transpirational cooling and high photosynthetic rates (Osborne *et al.*, 2004; Boyce, 2008; Brodribb *et al.*, 2010; Walls, 2011; Sack *et al.*, 2012).

Figs. 5(a)–5(c) show phase-contrast images and the phase-retrieved images of the control leaves (0 mT) and Figs. 6(a)–6(c) show the same for 200 mT treated leaves. The calculated values of the signal-to-noise ratio for phase-contrast and phase-retrieved images of the control leaf are 3.86 and 6.87, respectively. Similarly, for the 200 mT magneto-primed leaf the signal-to-noise ratio is 2 and 5.73 for phase-contrast and phase-retrieved images, respectively. There is an improvement in the signal-to-noise ratio in phase-retrieved images for leaves emerged from the remaining SMF (50, 100, 150, 250, 300) treatments (Figs. 7a–7e).

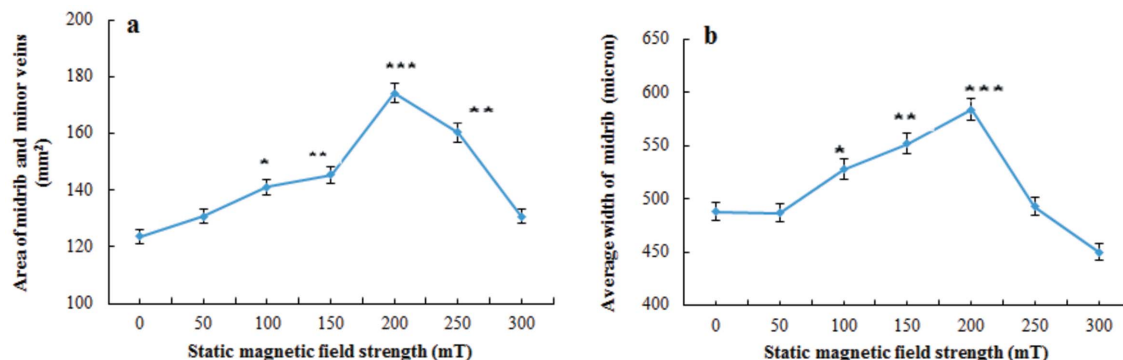


**Figure 4**  
 (a) Area of the midrib and minor veins and (b) average width of the midrib of middle leaflets of third trifoliate leaves of soybean plants emerged after pre-treatment of seeds with different SMF strength (0–300 mT). The error bars indicate  $\pm$  standard error for the mean. The values presented are significantly different at ( $**P < 0.01$ ,  $***P < 0.001$ ) from untreated seeds (Newman-Keulis multiple comparison test).

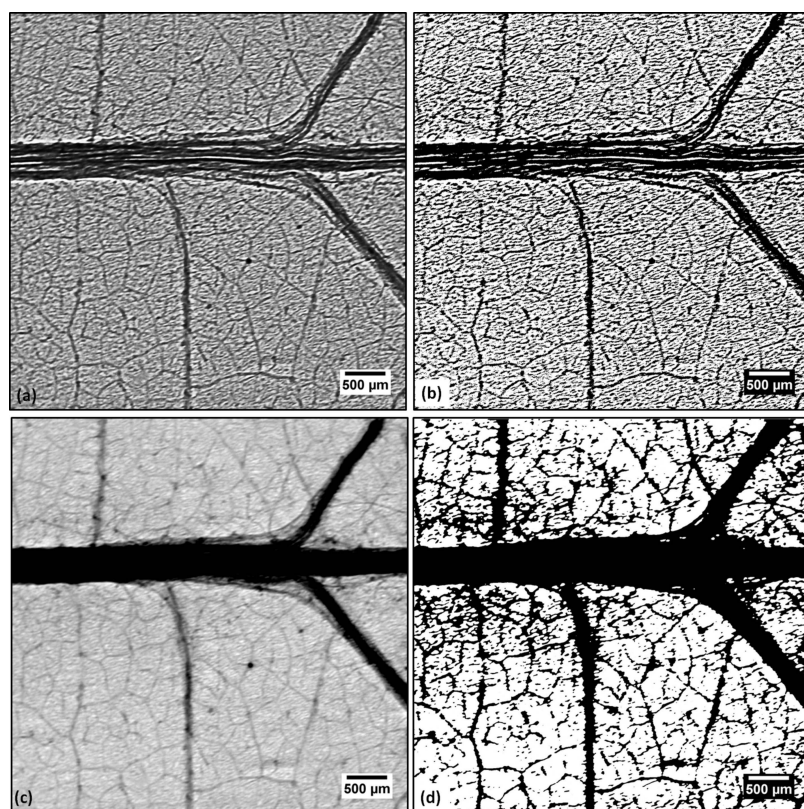


**Figure 5**  
 (a) Phase-contrast image of the control leaves; (b) segmented image of (a); (c) phase-retrieved image of (a); and (d) phase-retrieved image after segmentation.

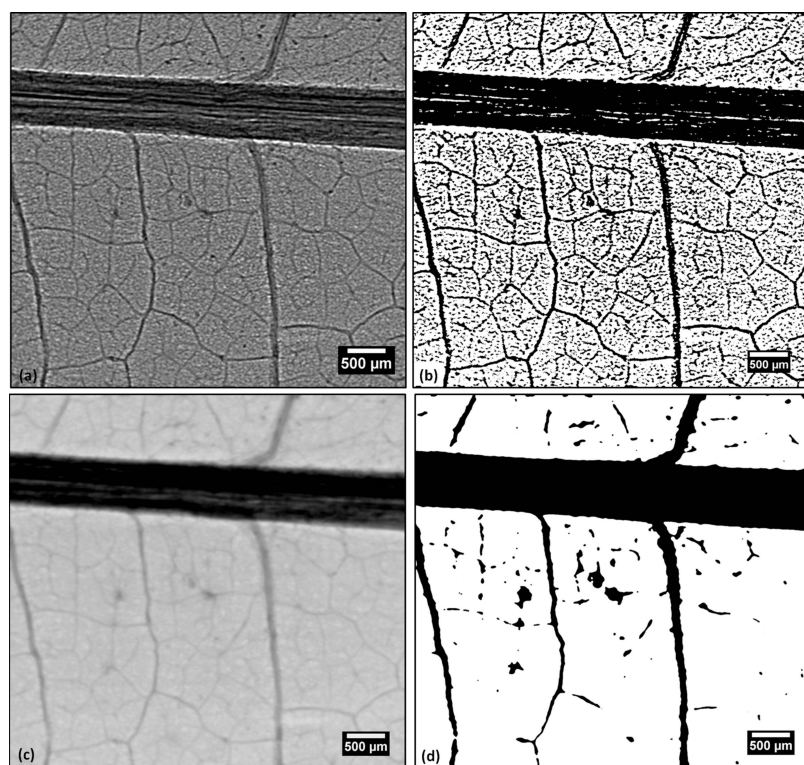


**Figure 6**  
 (a) Phase-contrast image of leaves grown from 200 mT magneto-primed seeds of soybean; (b) segmented image of (a); (c) phase-retrieved image of (a); and (d) segmented phase-retrieved image.

Comparison of phase-contrast images and the retrieved images of the control (Figs. 5*b* and 5*d*) shows an improved segmentation and visibility of 2° veins. Similar results were obtained on comparing the images for 200 mT treated leaves (Figs. 6*b* and 6*d*). The area of the leaf skeleton in the 1624 × 2040 pixel images was compared for the control and all the leaves grown after magneto-priming of seeds (Fig. 4*b*). Fig. 4*b*) shows the area of the midrib along with the 2° which are visible for the segmented images.

The phase-retrieved images for leaves grown with seeds magneto-primed with SMF strengths of 50, 100, 150, 250 and 300 mT are shown in Figs. 7*(a)–7(e)*. Fig. 8*(a)* (Fig. 5*c* shows the full image) and Fig. 8*(b)* (Fig. 6*c* shows the full image) are the zoomed phase-retrieved images of the region near the lower part of the midrib for the control and 200 mT SMF. Fig. 8*(c)* shows the zoomed phase-retrieved image after segmentation of the control leaves and Fig. 8*(d)* is for 200 mT leaves of soybean. The segmentation of the vascular region in Figs. 8*(c)–8(d)* shows the 2° and 3° veins. The distance between 3° veins (enclosed in the green square) which are visible in the segmented phase-retrieved images was found at three places (as shown by red lines in the images) using *ImageJ*. The average distance between 3° veins for control leaves is 300 μm and 793 μm for the 200 mT leaf. The larger separation of the 3° veins for 200 mT leaves shows enhancement of the leaf venation of soybean leaves as compared with the control.

The algorithm used for phase retrieval is valid if the object-to-detector distance fulfils the near-field condition (Weitkamp *et al.*, 2011). In the experimental data of leaves used for retrieval, although this condition is not satisfied, the retrieved images have a better signal-to-noise ratio and improved visibility of the veins. To the best of our knowledge this is the first report showing the effect of different strengths of SMF on leaf architectures and venation structures in soybean. Mousa *et al.* (2013) found that the anatomical stem parameters (*i.e.* stem diameter, stem cavity diameter, number of vascular bundle/cross section, vascular bundle diameter and vessel diameter) and the anatomical leaf parameters (*i.e.* lamina thickness, midrib thickness, midrib vascular bundle diameter and vessel diameter) of wheat plant were markedly enhanced by the different magnetic treatments at salinity level (10 dS m<sup>-1</sup>). Majd & Farzpour-machiani (2013) showed that magnetic field treated samples had a larger diameter, and more vascular bundles in roots and shoots and more xylem tissue in the root of *Vicia sativa*.

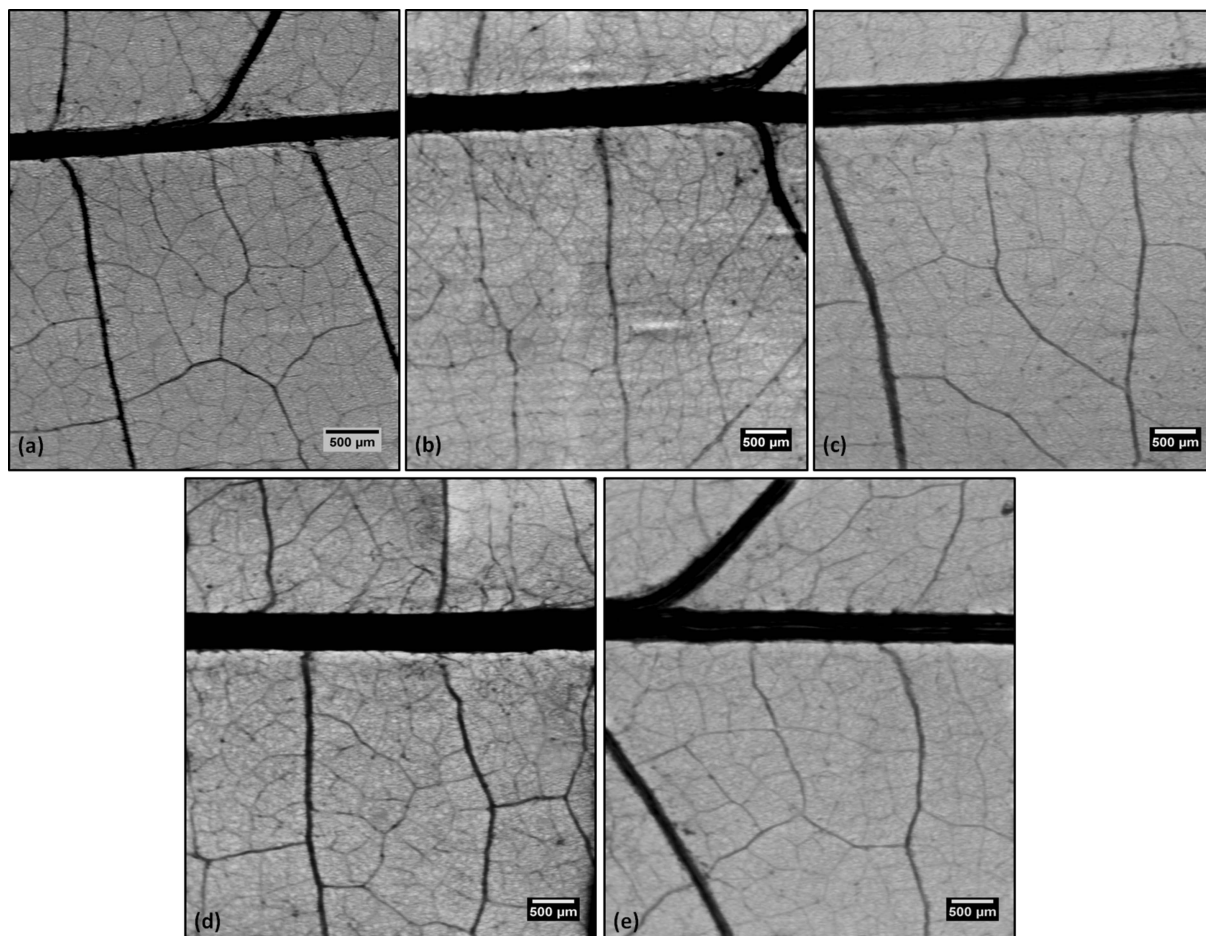


**Figure 7** Phase-retrieved images of leaves grown from magneto-primed seeds of soybean with different SMF strengths. (a) 50 mT; (b) 100 mT; (c) 150 mT; (d) 250 mT; (e) 300 mT.

### 9. Conclusion

X-ray phase contrast, a common technique for imaging of weakly absorbing samples, is used here to image leaves which comprise lighter elements, with the extension of the technique to phase retrieval from the intensity measurements. The method of phase retrieval demonstrated here with single-distance synchrotron-based phase images of leaves will ease the quantitative analysis. The data presented here provide a basis for evaluating the structural changes associated with increasing leaf photosynthetic rate and the stomatal conductance and the resultant impact on plant productivity after the SMF pretreatment of the seeds. The plants grown from seeds pre-treated with 200 mT SMF (1 h) have shown maximum enhancement in leaf area, width of midrib and rate of photosynthesis and stomatal conductance as compared with untreated controls (0 mT).

### Acknowledgements

Financial support by the Board of Research in Nuclear Sciences project, BARC, Mumbai (No. 2009/34/52/BRNS), and UGC-MANF for subsequent fellowship to AF and Department of Science Technology Women Scientists – A

Scheme (SR/WOS-A/LS-674/2012-G) to SK are thankfully acknowledged.

### References

Agrawal, A. K., Singh, B., Kashyap, Y. S., Shukla, M., Sarkar, P. S. & Sinha, A. (2015). *J. Synchrotron Rad.* **22**, 1531–1539.  
 Anand, A., Nagarajan, S., Verma, A., Joshi, D., Pathak, P. & Bhardwaj, J. (2012). *Indian J. Biochem. Biophys.* **49**, 63–70.  
 Baghel, L., Kataria, S. & Guruprasad, K. N. (2015). *Int. J. Trop. Agri.* **33**, 977–983.  
 Baghel, L., Kataria, S. & Guruprasad, K. N. (2016). *Bioelectromagnetics*, **37**, 455–470.  
 Belyavskaya, N. A. (2004). *Adv. Space Res.* **34**, 1566–1574.  
 Blonder, B., De Carlo, F., Moore, J., Rivers, M. & Enquist, B. J. (2012). *New Phytol.* **196**, 1274–1282.  
 Boyce, C. K. (2008). *Paleontolog. Soc. Papers.* **14**, 133–146.  
 Brodersen, C. R., Lee, E. F., Choat, B., Jansen, S., Phillips, R. J., Shackel, K. A., McElrone, A. J. & Matthews, M. A. (2011). *New Phytol.* **191**, 168–1179.  
 Brodribb, T. J., Feild, T. S. & Jordan, G. J. (2007). *Plant Physiol.* **144**, 1890–1898.  
 Brodribb, T. J., Feild, T. S. & Sack, L. (2010). *Funct. Plant Biol.* **37**, 488–498.  
 Camps-Raga, B., Gyawali, S. & Islam, N. E. (2009). *IEEE Trans. Dielec. Elec. Insul.* **16**, 1317–1321.

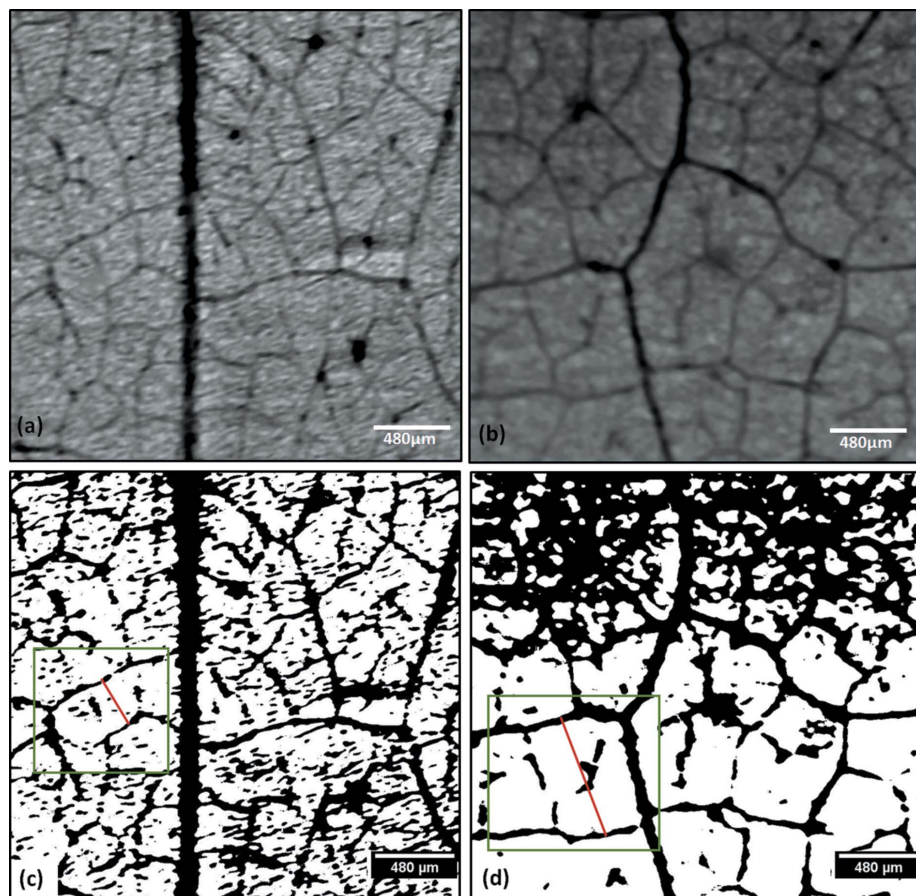


**Figure 8**

Zoomed images of the vascular network in the lower region near the midrib: (a) phase-contrast image of control leaves, (b) leaves grown from 200 mT magneto-primed seeds of soybean, (c) segmented phase-retrieved images for average distance between the 3° veins in the control, (d) segmented phase-retrieved images for average distance between the 3° veins in a leaf grown from magneto-primed seed with 200 mT magnetic field.

- Fatima, A., Kataria, S., Guruprasad, K. N., Agrawal, A. K., Singh, B., Sarkar, P. S., Shripathi, T., Kashyap, Y. & Sinha, A. (2016). *J. Synchrotron Rad.* **23**, 795–801.
- Florez, M., Carbonell, M. V. & Martinez, E. (2007). *Environ. Exp. Bot.* **59**, 68–75.
- Galland, P. & Pazar, A. (2005). *J. Plant Res.* **118**, 371–389.
- Galmés, J., Conesa, M. À., Ochogavía, J. M., Perdomo, J. A., Francis, D. M., Ribas-Carbó, M., Savé, R., Flexas, J., Medrano, H. L. & Cifre, J. (2011). *Plant Cell Environ.* **34**, 245–260.
- Kataria, S., Baghel, L. & Guruprasad, K. N. (2015). *Int. J. Trop. Agri.* **33**, 1–7.
- Majd, A. & Farzpourmachiani, S. (2013). *Global Plant Ecophysiol.* **3**, 87–95.
- Mayo, S. C., Chen, F. & Evans, R. (2010). *J. Struct. Biol.* **171**, 182–188.
- Mokso, R., Marone, F., Irvine, S., Nyvlt, M., Schwyn, D., Mader, K., Taylor, G. K., Krapp, H. G., Skeren, M. & Stamparoni, M. (2013). *J. Phys. D.* **46**, 494004.
- Mousa, E. M., Gendy, A. A., Maria, A. M. & Selim, A. D. (2013). *Minufiya J. Agri. Res.* **38**, 31–41.
- Muraji, M., Asai, T. & Tatebe, W. (1998). *Bioelectrochem. Bioenerg.* **44**, 271–273.
- Myers, G. R., Mayo, S. C., Gureyev, T. E., Pagannin, D. M. & Wilkins, S. W. (2007). *Phy. Rev. A*, **76**, 045804.
- Osborne, C. P., Beerling, D. J., Lomax, B. H. & Chaloner, W. G. (2004). *Proc. Natl Acad. Sci. USA*, **101**, 10360–10362.
- Paganin, D., Mayo, S. C., Gureyev, T. E., Miller, P. R. & Wilkins, S. W. (2002). *J. Microsc.* **206**, 33–40.
- Price, C. A., Symonova, O., Mileyko, Y., Hilley, T. & Weitz, J. S. (2011). *Plant Physiol.* **155**, 236–245.
- Rasband, W. S. (2012). *ImageJ*. US National Institutes of Health, Bethesda, Maryland, USA. <http://imagej.nih.gov/ij/>.
- Reina, F. G. & Pascual, L. A. (2001). *Bioelectromagnetics*, **22**, 589–595.
- Rolland-Lagan, A., Amin, M. & Pakulska, M. (2009). *Plant J.* **57**, 195–205.
- Roth-Nebelsick, A., Uhl, D., Mosbrugger, V. & Kerp, H. (2001). *Ann. Bot.* **87**, 553–566.
- Sack, L. & Holbrook, N. M. (2006). *Annu. Rev. Plant Biol.* **57**, 361–381.
- Sack, L., Scoffoni, C., McKown, A. D., Frole, K., Rawls, M., Havran, J. C., Tran, H. & Tran, T. (2012). *Nat. Commun.* **3**, 837.
- Shine, M. B. & Guruprasad, K. N. (2012). *Acta Physiol. Plant.* **34**, 255–265.
- Shine, M. B., Guruprasad, K. N. & Anand, A. (2011a). *Plant Signal. Behav.* **6**, 1635–1637.
- Shine, M. B., Guruprasad, K. N. & Anand, A. (2011b). *Bioelectromagnetics*, **32**, 474–484.
- Snigirev, A., Snigireva, I., Kohn, V., Kuznetsov, S. & Schelokov, I. (1995). *Rev. Sci. Instrum.* **66**, 5486–5492.
- Thomas, S., Anand, A., Chinnusamy, V., Dahiya, A. & Basu, S. (2013). *Acta Physiol. Plant.* **35**, 3401–3411.
- Vashisth, A. & Nagrajan, S. (2008). *Bioelectromagnetics*, **29**, 571–578.
- Walls, R. L. (2011). *Am. J. Bot.* **98**, 244–253.
- Weitkamp, T., Haas, D., Wegrzynek, D. & Rack, A. (2011). *J. Synchrotron Rad.* **18**, 617–629.
- Wilkins, S. W., Gureyev, T. E., Gao, D., Pogany, A. & Stevenson, A. W. (1996). *Nature (London)*, **384**, 335–338.
- Xu, F., Helfen, L., Moffat, A. J., Johnson, G., Sinclair, I. & Baumbach, T. (2010). *J. Synchrotron Rad.* **17**, 222–226.
- Zápražný, Z., Korytár, D., Mikulík, P. & Áč, V. (2013). *J. Appl. Cryst.* **46**, 933–938.
- Zimmermann, M. H. & Tomlinson, P. B. (1966). *Science*, **152**, 72–73.